Sound velocity measurements of hcp Fe-Si alloy at high pressure and high temperature by inelastic X-ray scattering

doi: 10.2138/am-2018-6072

Sound velocity measurements of hcp Fe–Si alloy at high pressure and high temperature by inelastic X-ray scattering

Revision 2

Takanori Sakairi[1], Tatsuya Sakamaki[1], Eiji Ohtani[1,2]*, Hiroshi Fukui[3,4], Seiji Kamada[5], Satoshi Tsutsui[6], Hiroshi Uchiyama[6], Alfred Q.R. Baron[4]

1. Department of Earth and Planetary Materials Science, Graduate school of Science, Tohoku University, Sendai 980-8578, Japan

2. V.S. Sobolev Institute of Geology and Mineralogy, Siberian Branch, Russian Academy of Sciences, Koptyuga Ave. 3, Novosibirsk 630090, Russia

3. Center for Novel Material Science under Multi-Extreme Conditions, Graduate School of Material Science, University of Hyogo, Kamigori, Hyogo 678-1297, Japan

4. Materials Dynamics Laboratory, RIKEN SPring-8 Center, Sayo, Hyogo 679-5148, Japan

5. Frontier Research Institute for Interdisciplinary Sciences, Tohoku University, Sendai 980-8578, Japan

6. Japan Synchrotron Radiation Research Institute (JASRI), Hyogo 679-5198, Japan

***Corresponding author**

Revise and resubmitted to Am. Mineralogist

Abstract

The sound velocity of hcp $Fe_{0.89}Si_{0.11}$ (Fe–6wt. % Si) alloy was measured at pressures from 45 to 84 GPa and temperatures of 300 and 1800 K using inelastic X-ray scattering (IXS) from laser-heated samples in diamond anvil cells (DACs). The compressional velocity (V_P) and density (ρ) of the Fe–Si alloy are observed to follow a linear relationship at a given temperature. For hcp $Fe_{0.89}Si_{0.11}$ alloy we found V_P = 1.030 (± 0.008) × ρ-1.45 (±0.08) + [3.8×10^{-5}(T-300)×(ρ-15.37)], including non-negligible temperature dependence. The present results of sound velocity and density of hcp $Fe_{0.89}Si_{0.11}$ alloy indicates that 3~6 wt. % of silicon in the inner core with additional amount of Ni can explain the compressional velocity (V_P) and density (ρ) of the "Preliminary Earth reference model" (PREM), assuming a temperature of 5500 K and that silicon is the only light element in the inner core

Keywords: Sound velocity, Fe-Si alloy, High pressure, High temperature, Inelastic X-ray scattering, Inner core, Birch's law, Silicon

Introduction

The profile of the density and sound velocity of the Earth's deep interior has been modeled by seismological observations leading to the creation of the Preliminary Earth reference model, PREM, [*Dziewonski and Anderson*, 1981]. The Earth's inner core is considered to be mainly composed of iron-nickel alloy with small amount of light elements to account for the core density deficit [*Birch*, 1964]. We can constrain the composition of the core by comparing sound velocity and density data of Fe and Fe alloys with PREM. Therefore, sound velocity measurements of Fe and Fe-light element alloys have been performed under high pressure conditions using various methods, such as shock wave experiments [e.g., *Brown and McQeen*, 1986], inelastic X-ray scattering (IXS) [e.g., *Antonangeli et al*., 2010; *Mao et al., 2012*; *Ohtani et al*., 2013; *Sakamaki et al*., 2016], nuclear resonance inelastic X-ray scattering (NRIXS or NIS) [e.g., *Lin et al*., 2003].

It is generally accepted that, as a first approximation, there is a linear relationship between density and sound velocity, i.e., Birch's law [*Birch*, 1961; *Antonangeli and Ohtani*, 2015]. We used the expression "Birch's law" for the linear dependence of the sound velocity on density at a constant temperature, even when the temperature effects are important. However, the effect of temperature on Birch's law is

not yet well understood. Thus additional data on temperature dependence, especially for Fe alloys with light impurities, are important to allow understanding of the core composition.

Silicon is one of the major candidates for light elements in the Earth's core. The sound velocity of Fe–Si alloy at room temperature has been measured by several methods such as NRIXS (NIS) [*Lin et al*., 2003] and IXS [*Badro et al*., 2007; *Mao et al*., 2012], however, the results have not been consistent. Using NRIXS (NIS) to investigate hcp $Fe_{0.85}Si_{0.15}$ alloy, *Lin et al*. [2003] reported that dissolution of silicon in metallic iron increases both the compressional velocity and shear velocity of iron alloys at high pressure. Using IXS to investigate FeSi at room temperature, *Badro et al*. [2007] suggested that the incorporation of small amounts of silicon, 2.3 wt. %, might account for the geophysical observations including the PREM sound velocity of the inner core. In contrast, the work of *Mao et al*. [2012] using IXS to investigate hcp $Fe_{0.85}Si_{0.15}$ alloy at 300 K suggests the PREM inner core matches a velocity profile of iron with 8 wt. % Si. On the other hand, *Liu et al.* [2016] suggested that the PREM inner core can be explained by 5 wt.% Si based on the combined measurements of IXS and NRIXS for hcp-Fe and hcp-$Fe_{0.868}Ni_{0.086}Si_{0.046}$ at room temperature and high pressure.

Sound velocity measurements of hcp Fe–Si alloy at high pressure and

temperature have not been reported yet and certainly may impact these discussions. Here we report the sound velocity of hcp $Fe_{0.89}Si_{0.11}$ (Fe–6wt.% Si) alloy up to 84 GPa and 1800 K based on IXS measurements, including the effect of temperature on the sound velocity of the alloy. In this context, we discuss the silicon content of the Earth's inner core.

Experimental procedure

Sample Environment

High pressure was generated by a symmetric-type DAC. The culet sizes of the diamond anvils were 200 and 300 μm, depending on the desired experimental pressures. The starting material used in this study was $Fe_{0.89}Si_{0.11}$ (Fe–6 wt. % Si alloy, 99.995% purity, Lot No. 20113-27-08-02A; Rare Metallic Co., Ltd). We confirmed that the alloy sample is homogeneous and has the composition with the accuracy within 0.5 wt. % by the FE-SEM (JEOL7001F) analyses. A thin foil of the starting material was made by compressing the alloy chip at room temperature by using opposite anvils (a cold compression technique) and by polishing it to a desired thickness. The sample foil was sandwiched between NaCl pellets, which worked as a pressure medium and thermal insulator. A rhenium gasket was indented to a thickness of 30–50 μm and a hole with a diameter in 80–100 μm was drilled to shape a sample chamber.

For high temperature experiments, the COMPAT double sided laser-heating system, which has been developed for IXS-LHDAC by *Fukui et al*. [2013], was used and the sample was heated from both sides using a fiber laser (λ= 1.070 μm). The temperature was monitored, and recorded every 30 min during heating. The temperature was determined by fitting Plank's formula to a spectrum of thermal radiation from the sample. The laser spot size in the sample was 20-25 μm in diameter as was reported by *Sakamaki et al.* [2016]. The temperature distribution within the heating spot was similar to that given in Figure S1 by *Sakamaki et al.* [2016].

The sample position was adjusted to the maximum intensity of the X-ray diffraction from the sample by changing its position. Once the sample and X-ray beam positions were fixed, we adjusted the laser beam position by observing the sample by using a CCD camera. We could easily monitor the laser beam position in the sample by the emission from the laser heated area. The emission was collected from the center of the emitted area in the sample. The experimental temperature was evaluated with the uncertainty of ±200 K by averaging the variation of temperature in the heating area during the IXS measurements.

Inelastic X-ray scattering at SPring-8

Sound velocity of Fe–Si alloy was measured using inelastic X-ray scattering at BL35XU [*Baron et al*., 2000] of SPring-8. Si (9 9 9) backscattering optics were used, providing an incident photon energy of 17.79 keV with an energy resolution of 2.8 meV full width at half-maximum (FWHM). The scattered X-rays were analyzed by 12 crystals, which are arranged in a 2-dimensional (3×4) array. The momentum transfer, $Q=2k_0\sin(2\theta/2)$, where k_0 is the wave vector of the incident photons and 2θ is the scattering angle, was selected by rotating the spectrometer arm in the horizontal plane. The X-ray beam size was focused to 16 μm×16 μm by a Kirkpatrick-Baez (KB) mirror pair [*Ishikawa* et al., 2013]. IXS was collected in the range of Q= 6.2–9.5 nm^{-1} at each pressure condition. The momentum resolution was set to about 0.4 nm^{-1} full width. Spectra were measured for about 8-12 hours at room temperature and 6-8 hours at high temperature. A shorter duration at high temperature was due to higher intensity of the IXS signals at higher temperature.

In order to calculate the density of Fe–Si alloy, *in-situ* X-ray diffraction patterns of samples were obtained using a flat panel detector (FP; C9732DK, Hamamatsu Photonics K.K.) at the same experimental conditions as IXS measurements. The distance between the sample and a FP detector was calibrated by collecting the diffraction pattern of CeO_2. The density of Fe–Si alloy was calculated based on lattice

parameters of Fe–Si alloy in the XRD pattern. The experimental pressure at room temperature was determined assuming that the parameters of the equation of state (K_0, K_0' and V_0) of hcp $Fe_{0.89}Si_{0.11}$ (Fe-6.0wt.%Si) is the same as those of Fe-6.5wt.%Si [*Tateno* et al., 2015]. At high temperature, parameters of thermal equation of state (θ_0, γ_0 and q) of Fe–9 wt. %Si alloy [*Fischer et al*., 2014] were used for the pressure estimation. Since the effect of Si dissolution on volume of Fe-Si alloy is very small [e.g., Fischer et al., 2014; Tateno et al., 2015; Sakai et al., 2014], the uncertainty of pressure at 84 GPa and 1800 K was estimated to be within 0.5 GPa (less than 1%) in this experiment. This uncertainty is smaller than the estimated pressure error from the pressure gradient in the cell. A typical X-ray diffraction pattern from the sample is shown in Fig.1. An example of the IXS spectrum collected at 84 GPa and 1800 K is shown in Fig. 2. The spectra are characterized by an elastic contribution centered at zero energy and inelastic contributions from Fe-Si alloy. As shown in Fig. 2, the spectra derived from the longitudinal acoustic (LA) phonons of Fe-Si alloy were observed. The LA mode of rhenium which was originated from gasket was also observed in this spectra. The energy positions of phonons were extracted by fitting the spectra data with a set of Lorentzian functions. In order to determine the compressional velocity (V_P), the phonon dispersion measured here was fitted using a sine function as shown below:

$$E\,[meV] = 4.192 \times 10^{-4} V_P\ [m/s] \times Q_{MAX}\ [nm^{-1}]\ \sin\ ((\pi/2)Q[nm^{-1}]\ /\ Q_{MAX}\ [nm^{-1}]) \quad (1)$$

where E and Q are the energy and the momentum transfer of the acoustic mode, and V_P is the compressional velocity of Fe–Si alloy in this study. Q_{MAX} corresponds to the first Brillouin zone edge [e.g., *Fiquet et al*., 2004]. V_P and Q_{MAX} were taken as free parameters.

The sample holes during compression shrank to around 40-60 μm at high pressure, and in some experiments in which the sample is close to the Re gasket, we observed signals from the gasket in XRD and IXS spectra (Figures 1 and 2) due to a tail of the X-ray beam. The pressure gradients in the cell using NaCl pressure medium were evaluated and given in Table 1. The pressure errors from the pressure scale are smaller than the errors due to present pressure errors. The IXS peaks came from the high temperature samples of FeSi alloy, in which the temperature distributions around the sample was homogeneous, therefore a similarity in the texture development with *Sakamaki et al.* [2016] holds in the present experiments.

Results

Sound velocity of Fe-Si alloy

IXS measurements were conducted in the pressure range from 45 to 84 GPa

and the temperatures of 300 K and 1800 K. The experimental conditions are summarized in Table 1. We conducted the experiments in the pressure and temperature conditions which correspond to the stability field of hcp phase of Fe-Si alloy because Earth's inner core is considered to be composed of the hcp phase [e.g., *Tateno et al.*, 2010]. Dispersion curves of Fe–Si alloy at each measurement were compiled in Fig. 3. The obtained density (ρ) and compressional velocity (V_P) *at various pressures and temperatures* were also shown in Table 1. We can see that V_P increases with increasing pressure.

Birch's law for hcp Fe–Si alloy

Fig. 4 shows the measured compressional velocity, V_P of the hcp Fe–Si alloy as a function of density. The V_P and density of hcp Fe–Si alloy showed a linear relationship i.e., Birch's law, in this study. In order to evaluate the effect of temperature on the sound velocity of hcp Fe–Si alloy, the V_P data at 300 K and 1800 K were fitted separately as a linear function of density, using Birch's law. The Birch's law of hcp Fe–6 wt. % Si ($Fe_{0.89}Si_{0.11}$) alloy at 300 K was obtained as shown below:

$$V_P = 1.030(\pm 0.008) \times \rho\text{-}1.45\ (\pm 0.08) \quad (2)$$

On the other hand, the Birch's law at 1800 K was expressed as follows:

$V_P = 1.087\ (\pm 0010) \times \rho\text{-}2.33\ (\pm 0.10)$ (3)

These relationships at 300 K and 1800 K indicate that the Birch's law for the hcp Fe–6 wt. % Si alloy has a clear temperature dependency as shown in Fig. 4. We then parameterize the temperature dependence as $V_P(\rho, T) = M\rho + B + A(T - T_0)(\rho - \rho^*)$, which was introduced by *Sakamaki et al.* [2016]. We choose T_0 to be 300K, so M and B are the coefficients of Birch's law at room temperature, while A and ρ^* include the temperature dependence. Thus, the high temperature Birch's law of hcp Fe–6 wt. % Si ($Fe_{0.89}Si_{0.11}$) can be expressed as follows:

$V_P = 1.030\ (\pm 0.008) \times \rho\text{-}1.45\ (\pm 0.08) + [3.8\times10^{-5}(T\text{-}300)\times(\rho\text{-}15.37)]$ (4)

The present modified Birch's law for hcp Fe-Si alloy obtained here indicates that the slope of the Birch's law for hcp Fe-Si is similar to that of hcp Fe [*Sakamaki et al.*, 2016]. On the other hand, Si alloying reduces the temperature effect of the modified Birch's law as shown in Fig. 5.

Discussion

In order to compare Birch's law of hcp Fe–Si alloy between this study and previous studies, the sound velocities of hcp Fe–Si alloy measured by the IXS method [*Badro et al*. 2007; *Mao et al*. 2012] and NRIXS method [*Lin et al*., 2003] are summarized in Fig.

4. Birch's law for $Fe_{0.85}Si_{0.15}$ alloy reported by *Lin et al.* [2003] by NRIXS is not consistent with that reported by *Mao et al.* [2012] for the same composition. This may be the effect of different experimental conditions (no pressure medium was used in NRIXS, whereas Ne or NaCl pressure medium was used for IXS) and/or data processing as V_p was deduced indirectly for the NRIXS using the Debye sound velocity, V_D, and bulk modulus, K_s. Given that IXS provides more direct measurements for V_p with, we expect, a lower deviatoric stress, we compare our work with Birch's law reported by *Mao et al.* [2012] using the IXS method for $Fe_{0.85}Si_{0.15}$ alloy. The slope of Birch's law in this study is in good agreement with IXS results reported by *Mao et al*. [2012]. The larger differences between our results and those for FeSi reported by *Badro et al*. [2007] are probably the result of the very large difference in composition and structure: FeSi used by Badro has a different structure from the hcp-$Fe_{0.89}Si_{0.11}$ alloy of the present work.

The X-ray diffraction pattern of hcp Fe-Si alloy sample shown in Fig,1 was similar to that of hcp Fe at high pressure and temperature [*Sakamaki et al.,* 2016]. Thus, the lattice preferred orientation of the present compressed sample of hcp Fe-Si alloy may be a similar magnitude to that of hcp Fe measured previously [*Sakamaki et al.*, 2016]. The diffraction pattern shows that the polycrystalline hcp Fe–Si alloy sample

218 preferentially aligned with c-axis parallel to the compressional axis under the uniaxially
219 compressed conditions. According to the previous calculations of *Vp* anisotropy
220 associated with the preferred orientation of hcp-Fe is less than 1.3 % [*Sakamaki et al.*,
221 2016]. According to the *ab-initio* calculations by *Tsuchiya and Fujibuchi* [2009] and
222 *Martorell et al*. [2016], elastic constants, Cij, of hcp Fe-Si alloys have similar
223 anisotropic properties as those of hcp Fe. Therefore, we do not expect to have a
224 significant impact on the present results on the sound velocity. *Tsuchiya and Fujibuchi*
225 (2009) reached the same conclusion that the compressional velocity (*Vp*) anisotropy is
226 negligible although 2-4 % of *Vs* anisotropy is expected at high pressure based on the
227 *ab-initio* calculation, although we need confirmation by more detailed ab-initio
228 calculations for hcp Fe-Si alloy.

229 According to the previous experimental and theoretical studies, the
230 compressional velocity, *Vp,* of bcc Fe-Si alloy is greater than that of bcc Fe at the same
231 pressure [*Liu et al*., 2014; *Tsuchiya and Fujibuchi*, 2009]. Although our compressional
232 velocity values, *Vp* for hcp $Fe_{0.89}Si_{0.11}$, are higher than those of pure hcp Fe at 300 K in
233 the density-*Vp* plane as shown in Figure 5, they are nearly the same as those of pure hcp
234 Fe [*Ohtani et al.*, 2013] at a constant pressure and 300 K, consistent with those of pure
235 hcp Fe, hcp $Fe_{0.85}Si_{0.15}$ [*Mao et al.*, 2012], hcp $Fe0_{.868}Ni0_{.086}Si_{0.046}$ [*Liu et al.*, 2016], and

236 the results of *ab-initio* calculation [T*suchiya and Fujibuchi,* 2009].

237 The *ab-initio* calculations for hcp Fe and hcp FeSi alloys [Figure 5 in *Martorell*
238 *et al.,* 2016] indicated that the density-*Vp* relation at a constant temperature (0 K) and
239 that at a constant pressure (360 GPa) are different with each other, i.e., there is a
240 temperature effect in the Birch's law as was indicated by *Sakamaki et al.* [2016]. Our
241 modified Birch's law expressions for hcp Fe and hcp $Fe_{0.89}Si_{0.11}$ alloy given in (4) and
242 (7) are consistent with those calculated by *Martorell et al.* [2016] and *Vochadlo et al.*
243 [2010]; the temperature effect on our fitting equation of the density–*Vp* relation at 360
244 GPa in this work is $dVp/d\rho$ =3.9 (km/sec)/(gcm^{-3}) for hcp-$Fe_{0.89}Si_{0.11}$, on the other hand,
245 the ab-initio calculation indicates that $dVp/d\rho$ =5.7 (km/sec)/(gcm^{-3}) for $Fe_{0.9375}Si_{0.0625}$
246 [*Martorell et al.,* 2016] and 3.0 (km/sec)/(gcm^{-3}) for pure hcp-Fe [*Vochadlo et al.,* 2010]
247 at a constant pressure of 360 GPa. *Martorell et al.* [2016] indicated that there is no
248 pre-melting behavior in the sound velocity at high temperature in hcp Fe–Si alloy. This
249 indicates that a linear temperature effect on the density–*Vp* relation expressed by our
250 equation (4) for hcp Fe–Si alloy can be used for extrapolation to the inner core
251 conditions.

252

253 **Implications: the amount of silicon in the Earth's inner core**

254 The present experimental results of compressional velocity, V_P, for hcp
255 $Fe_{0.89}Si_{0.11}$ (Fe–6 wt. % Si) alloy demonstrated that Birch's law for Fe–Si alloys with the
256 hcp structure has a clear temperature dependency as shown in Equation (4). Therefore,
257 it may not be appropriate to ignore the effect of temperature on Birch's law at very high
258 temperature of the inner core estimated to be 5000 K–6000 K [e.g., *Terasaki et al*.,
259 2011]. In order to estimate the amount of silicon in the Earth's inner core, we adopted
260 a linear mixing model, which was used by some previous authors [e.g., *Antonangeli et*
261 *al*., 2010; *Badro et al*., 2007]. In this model, the average density ρ and sound velocity
262 V_P of a two-component ideal mixture are given as follows:

263 $$\rho = x\rho_{Fe\text{-}Si} + (1\text{-}x)\,\rho_{Fe} \qquad (5)$$

264 and

265 $$V_P = V_{Fe\text{-}Si}V_{Fe}/[(1\text{-}x)V_{Fe\text{-}Si} + xV_{Fe}] \qquad (6)$$

266 Where, x is the volume fraction of hcp $Fe_{0.89}Si_{0.11}$ alloy. The average density ρ and
267 sound velocity V_P were assigned to those of the inner core derived from the PREM
268 [*Dziewonski and Anderson*, 1981]. The temperature at ICB was assumed to be 5500 K
269 [e.g., *Terasaki et al*., 2011]. The temperature at the center of the core (CC) is assumed
270 to be the same as that at ICB [*Brown and McQueen*, 1986]. ρ_{Fe} at high pressure and
271 temperature conditions corresponding to the inner core was estimated by using thermal

272 equation of state of hcp Fe [*Sakai et al*. 2014] and V_{Fe} was calculated based on our
273 modified Birch's law of iron which was proposed by *Sakamaki et al*. [2016]. According
274 to the modified Birch's law which was proposed by *Sakamaki et al*. [2016], the equation
275 for hcp Fe can be expressed as follows:

276 $V_{Fe} = 1.160\ (\pm 0.025) \times \rho\text{-}3.43\ (\pm 0.29) + [7.2\times10^{-5}\times(T\text{-}300)\times(\rho\text{-}14.2)]$ (7)

277 For the relation between $\rho_{Fe\text{-}Si}$ and $V_{Fe\text{-}Si}$, we used the equation of modified Birch's law
278 for hcp $Fe_{0.89}Si_{0.11}$ alloy shown in equation (4) obtained in the present study. The
279 densities of hcp $Fe_{0.89}Si_{0.11}$ alloy at the ICB and CC (center of the core) conditions were
280 calculated by the equation of state assuming that the parameters of the equation of state
281 (K_0, K_0' and V_0) is the same as that of Fe-6.5wt.%Si [*Tateno* et al., 2015] combined with
282 parameters of the thermal equation of state (θ_0, γ_0 and q) of Fe–9 wt. %Si alloy [*Fischer*
283 *et al*., 2014].

284 Fig. 5 summarizes sound velocities of pure hcp Fe and hcp Fe–Si alloy as a
285 function of density up to the temperature of ICB and CC, 5500 K, estimated by using
286 the equation (4), the modified Birch's law for the hcp Fe-Si alloy, and equation (7) for
287 pure hcp Fe. Fig. 6 shows the comparison between the compressional velocity V_P of the
288 linear mixing of hcp Fe and hcp $Fe_{0.89}Si_{0.11}$ (Fe–6 wt. % Si) and PREM at ICB (330
289 GPa) and CC (center of the core; 360 GPa) conditions as a function of density. The

290 temperature at CC is assumed to be the same that at ICB [*Brown and McQueen*, 1986].
291 From the data set of Equations (5) and (6) and considering the compressional velocity
292 V_P and density errors of PREM [*Masters*, 1979], the volume fraction of hcp $Fe_{0.89}Si_{0.11}$
293 alloy *x* was determined to be 0.5~1.0, i.e., 3~6 wt. % of silicon both for the ICB and CC
294 conditions. The present result indicates that an iron alloy with 3~6 wt. % of silicon can
295 explain the properties of the PREM inner core assuming that the light element in the
296 inner core is only silicon. This estimated value of silicon in the inner core is higher
297 compared to previous IXS studies [2.0 wt.% Si, *Antonangeli et al*., 2010; 2.3 wt.% Si,
298 *Badro et al*., 2007], and lower than the value, 8 wt.% Si, estimated by *Mao et al.* [2012].
299 3~6 wt. % of silicon determined from IXS measurements in this study may be the upper
300 bound of the amount of silicon in the Earth's inner core because other light elements
301 such as sulfur could be present in the inner core.

302 Recently *Martorell et al.* [2016)] reached a different conclusion, i.e., Fe-Si
303 alloy provides *Vp* higher than that of the PREM inner core based on their *ab-initio*
304 calculation. The present *Vp* for $Fe_{0.89}Si_{0.11}$ is significantly smaller than that calculated by
305 *Martorell et al.* [2016] resulting in different arguments on the effect of Si dissolution in
306 the inner core, i.e., our results revealed that the effect of Si can explain the density and
307 sound velocity of the PREM inner core. Our result on *Vp* is also consistent with the

experimental results by *Mao et al.* [2012] and *Liu et al.* [2016] at 300 K and the *ab-initio* calculation by *Tsuchiya and Fujibuchi* [2009] at 0 K, whereas *Vp* calculated by *Martorell et al.* [2016] at 0 K is significantly higher than the other results. On the other hand, the density value of $Fe_{0.89}Si_{0.11}$ extrapolated to 5500 K and 360 GPa in our experiments is consistent with that calculated at 360 GPa and 5500 K by *Martorell et al.* [2016], and is also consistent with the equation of state of Fe-Si alloys determined by *Tateno et al.* [2015], *Fischer et al.* [2014] and that calculated by *Tsuchiya and Fujibuchi* [2009].

The Earth's core is considered to contain about 5wt.% of Ni [*McDonough*, 2003]. If we consider an additional element, Ni, we can better match our model with the PREM inner core. The effect of Ni-alloying increases density of hcp-Fe, and it decreases slightly the sound velocity based on the sound velocity and density measurements of $Fe_{0.92}Ni_{0.08}$ [Lin et al., 2003; Sakai et al., 2014] and *ab-initio* calculations of Fe-Ni alloy and pure Ni [*Martorell et al.*, 2013a]. We estimated density and *Vp* of hcp $Fe_{0.92}Ni_{0.08}$ at 330 GPa and 360 GPa at 5500 K based on the temperature and pressure dependencies of hcp-Fe [*Sakamaki et al.*, 2016; *Martorell et al.*, 2013b] and plotted in Fig. 6. Based on these extrapolated values of density and *Vp* for hcp Fe, hcp $Fe_{0.89}Si_{0.11}$ and hcp $Fe_{0.92}Ni_{0.08}$, and the compressional velocity-density systematics

on compositional change [e.g., Liebermann and Ringwood, 1973], the PREM inner core can be explained by Ni bearing iron silicide with a composition of 3~6 wt.% Si and 0~6 wt.% Ni at ICB. On the other hand, the center of the inner core contains a similar Si content of 3~6 wt.% but it might contain a slightly higher content of Ni, 0~8 wt.% which may be better matching with the PREM inner core at its center although it is not definite due to a large uncertainty of the sound velocity of hcp Fe–Ni alloy at the inner core conditions and the density of the PREM inner core. We need further accurate experimental works under the inner core conditions and the seismic models to confirm the compositional gradient in the inner core.

Acknowledgments:

This work was supported by JSPS KAKENHI Grant Numbers 15H05748 to E.O. and 26247089 and 16H01112 to T. Sakamaki. This work was also supported partly by the Ministry of Education and Science of the Russian Federation (project 14.B25.31.0032) to E.O. T. Sakairi gratefully acknowledges JSPS for providing a research fellowship. The synchrotron radiation experiments were performed under contracts of the SPring-8 (proposal nos. 2012A1255, 2012B1439, 2013A1377, 2013A1492, 2013B1078, 2013B1094, 2014A1100, 2014B1269, 2014B1465, 2015A1539, 2015A1627, 2015B1202 and 2015B1334).

344

345 **References**

346 Antonangeli, D. and Ohtani, E. (2015) Sound velocity of hcp-Fe at high pressure:
347 experimental constraints, extrapolations and comparison with seismic models.
348 Progress in Earth and Planetary Science, 2:3 DOI 10.1186/s40645-015-0034-9

349 Antonangeli, D., Occelli, F., Requardt, H., Badro, J., Fiquet, G., and Krisch, M. (2004)
350 Elastic anisotropy in textured hcp-iron to 112 GPa from sound wave propagation
351 measurements. Earth and Planetary Science Letters, 225, 243–251.

352 Antonangeli, D., Siebert, J., Badro, J., Farber, D.L., Fiquet, G., Morard, G., and
353 Ryerson, F.J. (2010) Composition of the Earth's inner core from high-pressure
354 sound velocity measurements in Fe–Ni–Si alloys. Earth and Planetary Science
355 Letters, 295, 292–296.

356 Antonangeli, D., Komabayashi, T., Occelli, F., Borissenko, E., Walters, A.C., Fiquet, G.,
357 and Fei, Y. (2012) Simultaneous sound velocity and density measurements of hcp
358 iron up to 93 GPa and 1100 K: An experimental test of the Birch's law at high
359 temperature. Earth and Planetary Science Letters, 331, 210–214.

360 Badro, J., Fiquet, G., Guyot, F., Gregoryanz, E., Occelli, F., Antonangeli, D., and
361 d'Astuto, M. (2007) Effect of light elements on the sound velocities in solid iron:

implications for the composition of Earth's core. Earth and Planetary Science Letters, 254, 233–238.

Birch, F. (1961) Composition of the Earth's Mantle. Geophysical Journal International, 4, 295–311.

Birch, F. (1964) Density and composition of mantle and core. Journal of Geophysical Research, 69, 4377–4388.

Baron, A.Q.R., Tanaka, Y., Goto, S., Takeshita, K., Matsushita, T., and Ishikawa D. (2000) An X-ray scattering beamline for studying dynamics. Journal of Physics and Chemistry of Solids, 61, 461–465.

Brown, J.M. and McQueen, R.G. (1986) Phase transitions Grüneisen parameter and elasticity for shocked iron between 77 GPa and 400 GPa. Journal of Geophysical Research, 91, 7485–7494.

Dziewonski, A.M. and Anderson, D.L. (1981) Preliminary reference Earth model. Physics of the Earth and Planetary Interiors, 25, 297–356.

Fiquet, G., Badro, J., Guyot, F., Bellin, C., Krisch, M., Antonangeli, D., Requardt, H., Mermet, A., Farber, D., Aracne-Ruddle, C., and Zhang, J. (2004) Application of inelastic X-ray scattering to the measurements of acoustic wave velocities in geophysical materials at very high pressure. Physics of the Earth and Planetary

380 Interiors, 143-144, 5–18.

381 Fischer, R. A., Campbell, A.J., Caracas, R., Reaman, D.M., Heinz, D.L., Dera, P., and
382 Prakapenka, V.B. (2014) Equation of state in the Fe–FeSi system at high pressures
383 and temperatures. Journal of Geophysical Research, 119, 2810–2817.

384 Fukui, H., Sakai, T., Sakamaki, T., Kamada, S., Takahashi, S., Ohtani, E., and Baron
385 A.Q.R. (2013) A compact system for generating extreme pressures and
386 temperatures: An application of laser-heated diamond anvil cell to inelastic X-ray
387 scattering. Review of Scientific Instruments, 84, 113902.

388 Ishikawa, D., Uchiyama, H., Tsutsui, S., Fukui, H., and Baron, A.Q.R. (2013)
389 Compound focusing for hard-X-ray inelastic scattering. In: Proceedings of SPIE
390 8848, Advances in X-ray/EUV Optics and Components VIII, 88489F.

391 Liebermann, R.C. and Ringwood, A.E. (1973) Birch's law and polymorphic phase
392 transformations. Journal of Geophysical Research, 78, 6926-6932.

393 Lin, J.F., Struzhkin, V.V., Sturhahn, W., Huang, E., Zhao, J., Hu, M.Y., Alp, E.E., Mao,
394 H.K., Boctor, N., and Hemley R.J. (2003) Sound velocities of iron–nickel and iron–
395 silicon alloys at high pressures. Geophysical Research Letters, 30, 2112,
396 doi:10.1029/2003GL018405

397 Liu, J., Lin, J.F., Alatas, A., and Bi, W. (2014) Sound velocities of bcc-Fe and $Fe_{0.85}Si_{0.15}$

398 alloy at high pressure and temperature. Physics of the Earth and Planetary Interiors,
399 233, 24–32.
400 Liu, J., Lin, J.F., Alatas, A., Hu, M.Y., Zhao, J., and Dubrovinsky, L. (2016) Seismic
401 parameters of hcp-Fe alloyed with Ni and Si in the Earth's inner core. Journal of
402 Geophysical Research, 121, 610-623.
403 Mao, Z., Lin, J.F., Liu, J., Alatas, A., Gao, L., Zhao, J., and Mao H.K. (2012), Sound
404 velocities of Fe and Fe-Si alloy in the Earth's core. Proceedings of the National
405 Academy of Sciences of the United States, 109, 10239–10244.
406 Martorell, B., Brodholt, J.B., Wood, I.G., and Vočadlo, L. (2013a) The effect of nickel
407 on the properties of iron at the conditions of Earth's inner core: *Ab initio*
408 calculations of seismic wave velocities of Fe-Ni alloys. Earth and Planetary Science
409 Letters, 356, 143-151.
410 Martorell, B., Vočadlo, L., Brodholt, J.B., and Wood, I.G. (2013b) Strong premelting
411 effect in the elastic properties of hcp-Fe under inner-core conditions. Science, 342,
412 466-468.
413 Martorell, B., Wood, I.G., Brodholt, J.B., and Vočadlo, L. (2016) The elastic properties
414 of hcp-$Fe_{1-x}Si_x$ at Earth's inner-core conditions. Earth and Planetary Science Letters,
415 451, 89-96.

Masters, G. (1979), Observational constraints on the chemical and thermal structure of the earth's deep interior. Geophysical Journal International, 57, 507–534.

McDonough, W. F. (2003) Compositional model for the Earth's core. In R. W. Carlson, Ed., Treatise of Geochemistry, 2, p. 547–568, Elsevier-Pergamon, Oxford.

Ohtani, E., Shibazaki, Y., Sakai, T., Mibe, K., Fukui, H., Kamada, S., Sakamaki, T., Seto, Y., Tsutsui, S., and Baron A.Q.R. (2013) Sound velocity of hexagonal close-packed iron up to core pressures. Geophysical Research Letters, 40, 5089–5094.

Ohtani, E., Mibe, K., Sakamaki, T., Kamada, S., Takahashi, S., Fukui, H., Tsutsui, S., and Baron, A.Q.R. (2015) Sound velocity measurement by inelastic X-ray scattering at high pressure and temperature by resistive heating diamond anvil cell. Russian Geology and Geophysics, 56, 1-2, 190-195.

Sakamaki, T., Ohtani, E., Fukui, H., Kamada, S., Takahashi, S., Sakairi, T., Takahata, A., Sakai, T., Tsutsui, S., Ishikawa, D., Shiraishi, R., Seto, Y., Tsuchiya, T., and Baron, A.Q.R. (2016) Constraints on the Earth's inner core composition inferred from measurements of the sound velocity of hcp-iron in extreme conditions. Science Advances, 2: e1500802. DOI: 10.1126/sciadv.1500802

Sakai, T., Takahashi, S., Nishitani, N., Mashino, I., Ohtani, E., and Hirao, N. (2014)

Equation of state of pure iron and $Fe_{0.9}Ni_{0.1}$ alloy up to 3 Mbar, Physics of the Earth and Planetary Interiors, 228, 114–126.

Tateno, S., Hirose, H., Ohishi, Y., and Tatsumi, Y. (2010) The structure of iron in Earth's inner core. Science, 330, 359–361.

Tateno, S., Kuwayama, Y., Hirose, H., and Ohishi, Y. (2015) The structure of Fe-Si alloy in Earth's inner core. Earth and Planetary Science Letters, 418, 11–19.

Terasaki, H., Kamada, S., Sakai, T., Ohtani, E., Hirao, N., and Ohishi, Y. (2011) Liquidus and solidus temperature of a Fe–O–S alloy up to the pressures of the outer core: Implication for the thermal structure of the Earth's core. Earth and Planetary Science Letters, 232, 379–392.

Tsuchiya, T. and Fujibuchi, M. (2009) Effects of Si on the elastic property of Fe at Earth's inner core pressures: First principle study. Physics of the Earth and Planetary Interiors, 174, 212-219.

Figure Captions

Fig. 1. Typical 2D image of an X-ray diffraction pattern collected at 50 GPa and 1800 K. The diffraction lines from hcp Fe–Si alloy and Re are observed.

Fig. 2. A typical IXS spectrum of hcp $Fe_{0.89}Si_{0.11}$ at 84 GPa and 1800 K. The peak at

zero energy is from elastic scattering. Curves are individual contributions (green: elastic scattering, red: LA phonons of hcp $Fe_{0.89}Si_{0.11}$ sample, blue: rhenium), fitting the experimental data with Lorentzian functions.

Fig. 3. Dispersion curves obtained at 300 K and 1800 K in the pressure range 45–84 GPa.

Fig. 4. The compressional velocity V_P of $Fe_{0.89}Si_{0.11}$ (Fe-6wt.%Si) as a function of density. Blue solid diamond symbols show the present data of V_P at 300 K. Red solid circle symbols show our data measured at 1800 K. The blue line represents the Birch's law at 300 K, whereas the red line shows the Birch's law at 1800 K. The green dashed line with open green circles shows the IXS results for hcp-$Fe_{0.85}Si_{0.15}$ by *Mao et al.* [2012]. The purple dashed line with solid triangles shows the results by *Badro et al.* [2007] for FeSi alloy determined by IXS. The orange dashed line with orange solid triangles shows the results using NRIXS by *Lin et al.* [2003].

Fig. 5. Comparison of Birch's law of hcp $Fe_{.89}Si_{0.11}$(Fe–6wt.%Si alloy) and hcp-Fe. A blue line with blue triangles and a red line with red circles show the Birch's law for hcp

471 $Fe_{.89}Si_{0.11}$alloy at 300 K and 1800 K in this study, respectively. Solid square symbols
472 represent the density and V_P of PREM [*Dziewonski and Anderson*, 1981]. The black
473 cross line indicates the Birch's law for hcp $Fe_{.89}Si_{0.11}$ alloy extrapolated to 5500 K,
474 whereas the pink cross line indicates that for pure hcp-Fe extrapolated to 5500 K
475 [*Sakamaki et al*., 2016]. The Birch's relationship for pure hcp-Fe at 300 K [*Antonangeli*
476 *and Ohtani*, 2015] is shown as an orange dashed line. The errors for the Birch's law of
477 hcp $Fe_{.89}Si_{0.11}$ at 5500 K are shown as the grey shaded areas.
478
479 **Fig. 6.** The expected compressional velocity, *Vp*, of hcp Fe, hcp $Fe_{.89}Si_{0.11}$(Fe–6wt. %Si
480 alloy), hcp $Fe_{0.92}Ni_{0.08}$ and PREM inner core as a function of density at inner core
481 conditions (330-360 GPa and 5500 K). Stars indicate velocity and density at the ICB
482 condition (330-360 GPa and 5500 K). The *Vp* and density for hcp Fe were based on
483 *Sakamaki et al.* [2016], those for hcp $Fe_{.89}Si_{0.11}$ were based on the present measurements,
484 and those for hcp $Fe_{0.92}Ni_{0.08}$ were based on *Lin et al.* [2003]. We estimated the Si and
485 Ni contents in iron alloy based on the compressional velocity-density systematics on
486 compositional change [e.g., Liebermann and Ringwood, 1973]. The PREM inner core
487 can be explained by Ni bearing iron silicide with a composition of 3~6 wt.% Si and 0~6
488 wt.% Ni at ICB. Whereas, the center of the inner core has a similar Si content of 3~6

wt.% and a Ni content of 0~8 wt.%.

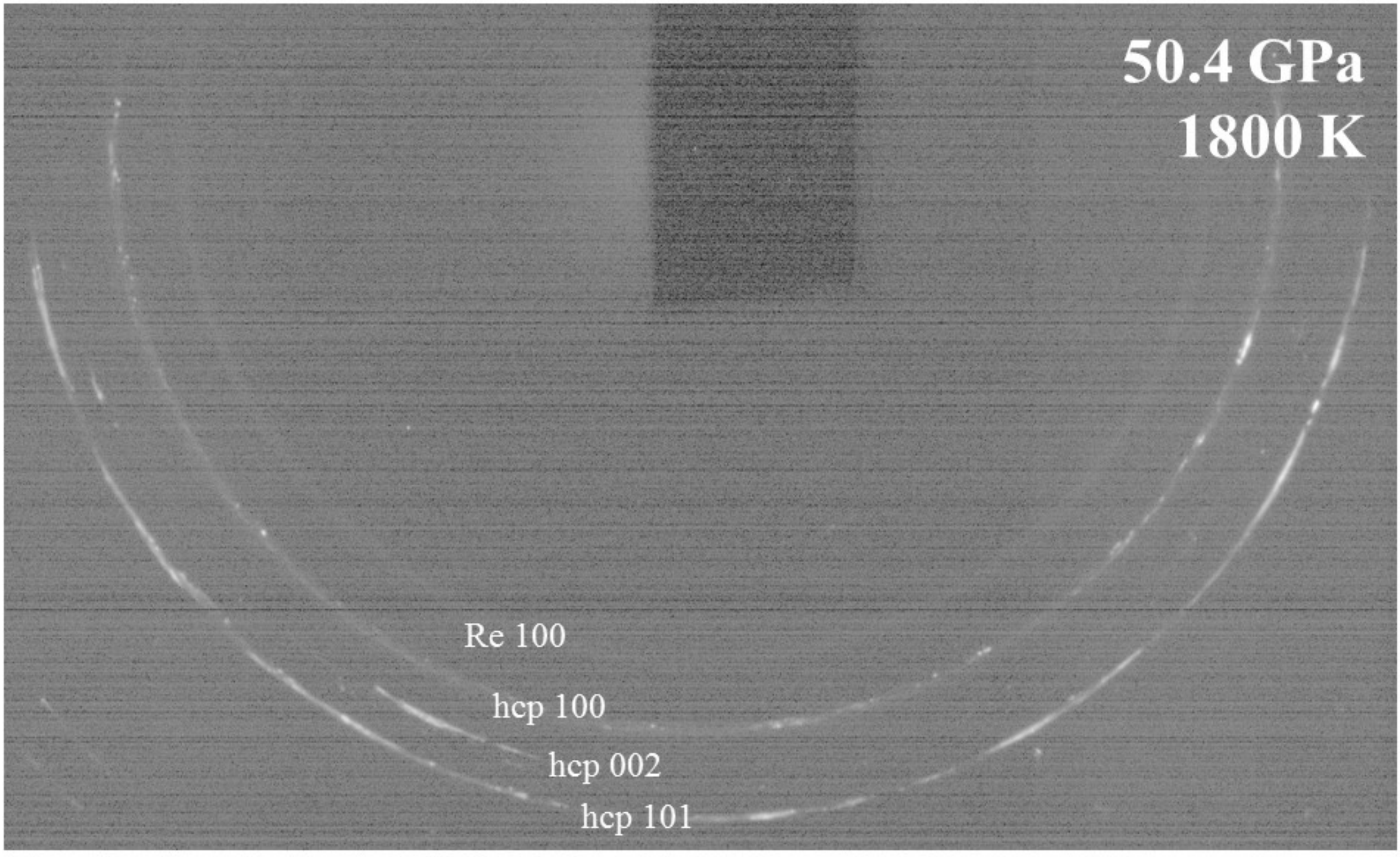

Figure 1

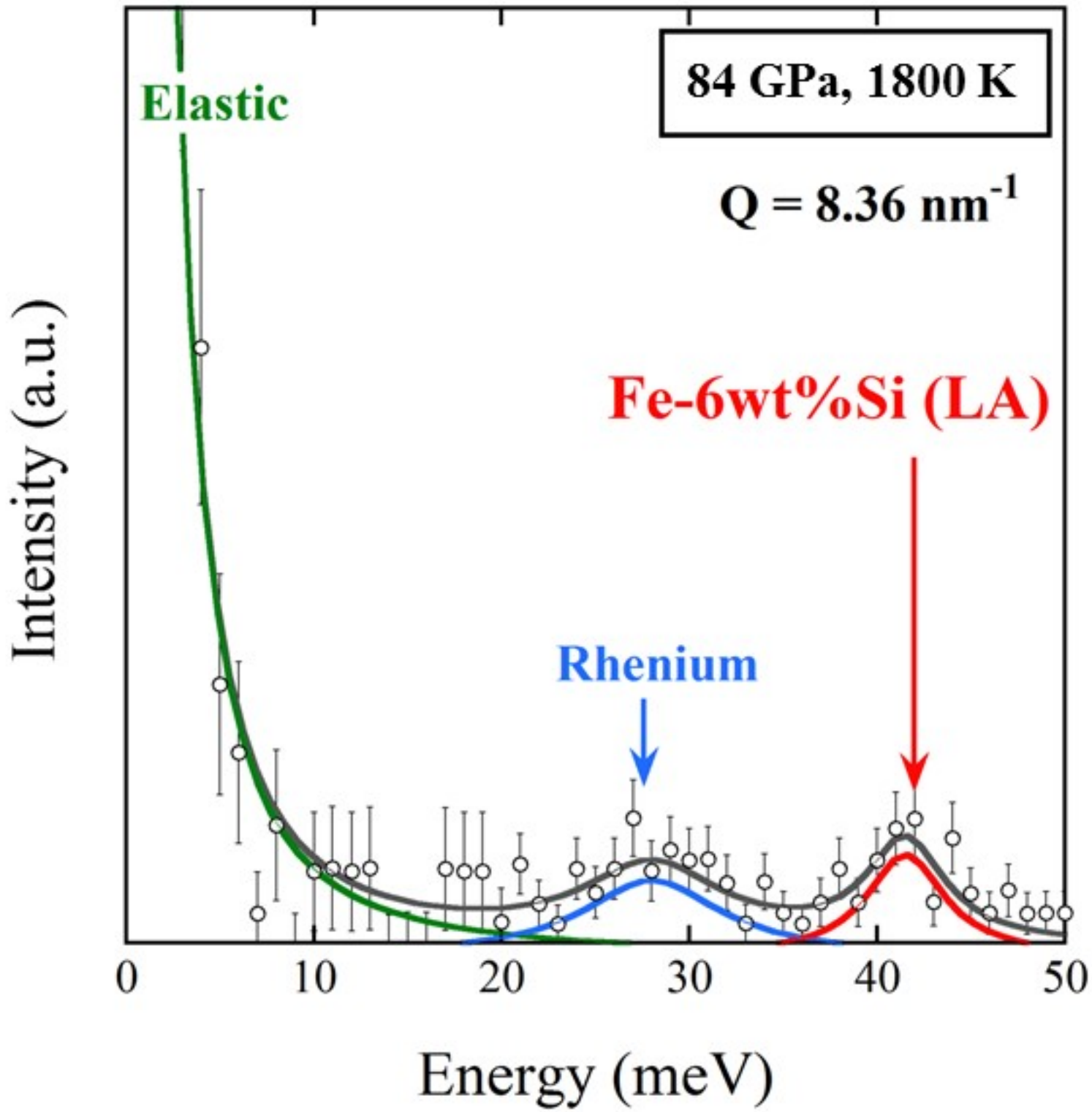
84 GPa, 1800 K
Q = 8.36 nm-1
Elastic
Fe-6wt%Si (LA)
Rhenium
Intensity (a.u.)
0
10
20
30
40
50
Energy (meV)

Figure 2

Figure 3

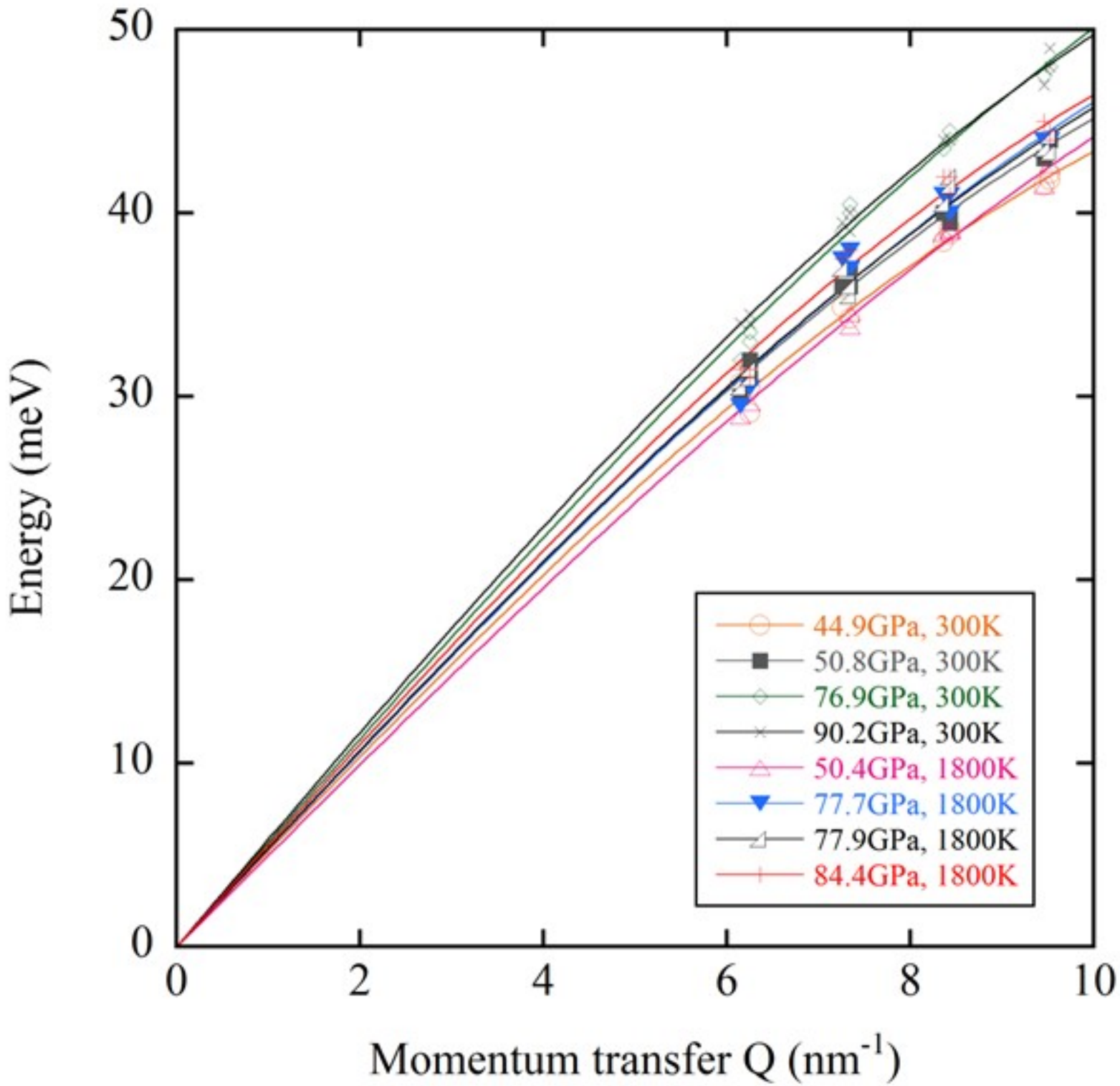
Energy (meV)
Momentum transfer Q (nm^{-1})
0
10
20
30
40
50
0
2
4
6
8
10
44.9GPa, 300K
50.8GPa, 300K
76.9GPa, 300K
90.2GPa, 300K
50.4GPa, 1800K
77.7GPa, 1800K
77.9GPa, 1800K
84.4GPa, 1800K

Figure 4

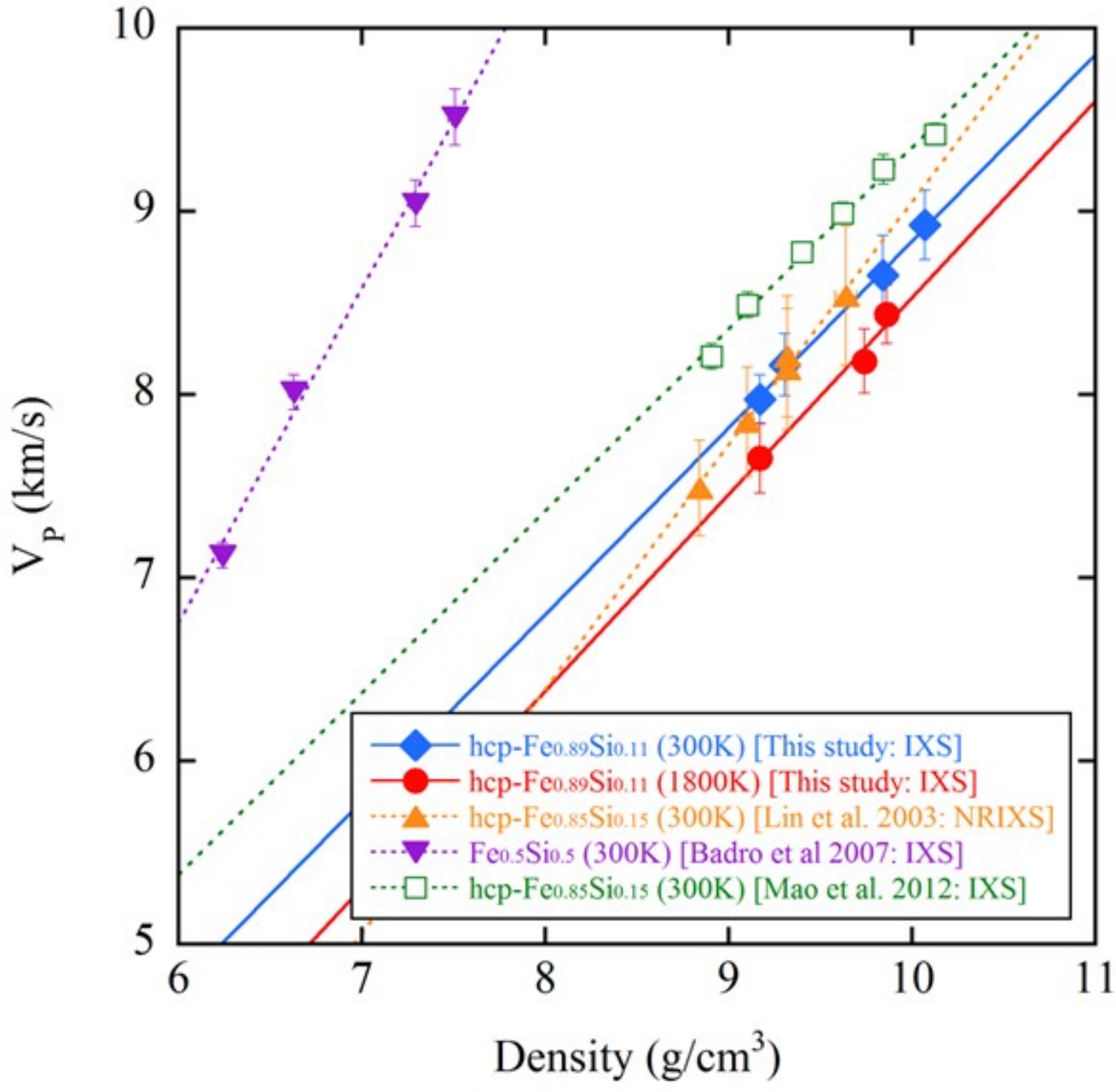
10
9
8
7
6
5
6
7
8
9
10
11
V_P (km/s)
Density (g/cm^3)
hcp-Fe0.89Si0.11 (300K) [This study: IXS]
hcp-Fe0.89Si0.11 (1800K) [This study: IXS]
hcp-Fe0.85Si0.15 (300K) [Lin et al. 2003: NRIXS]
Fe0.5Si0.5 (300K) [Badro et al 2007: IXS]
hcp-Fe0.85Si0.15 (300K) [Mao et al. 2012: IXS]

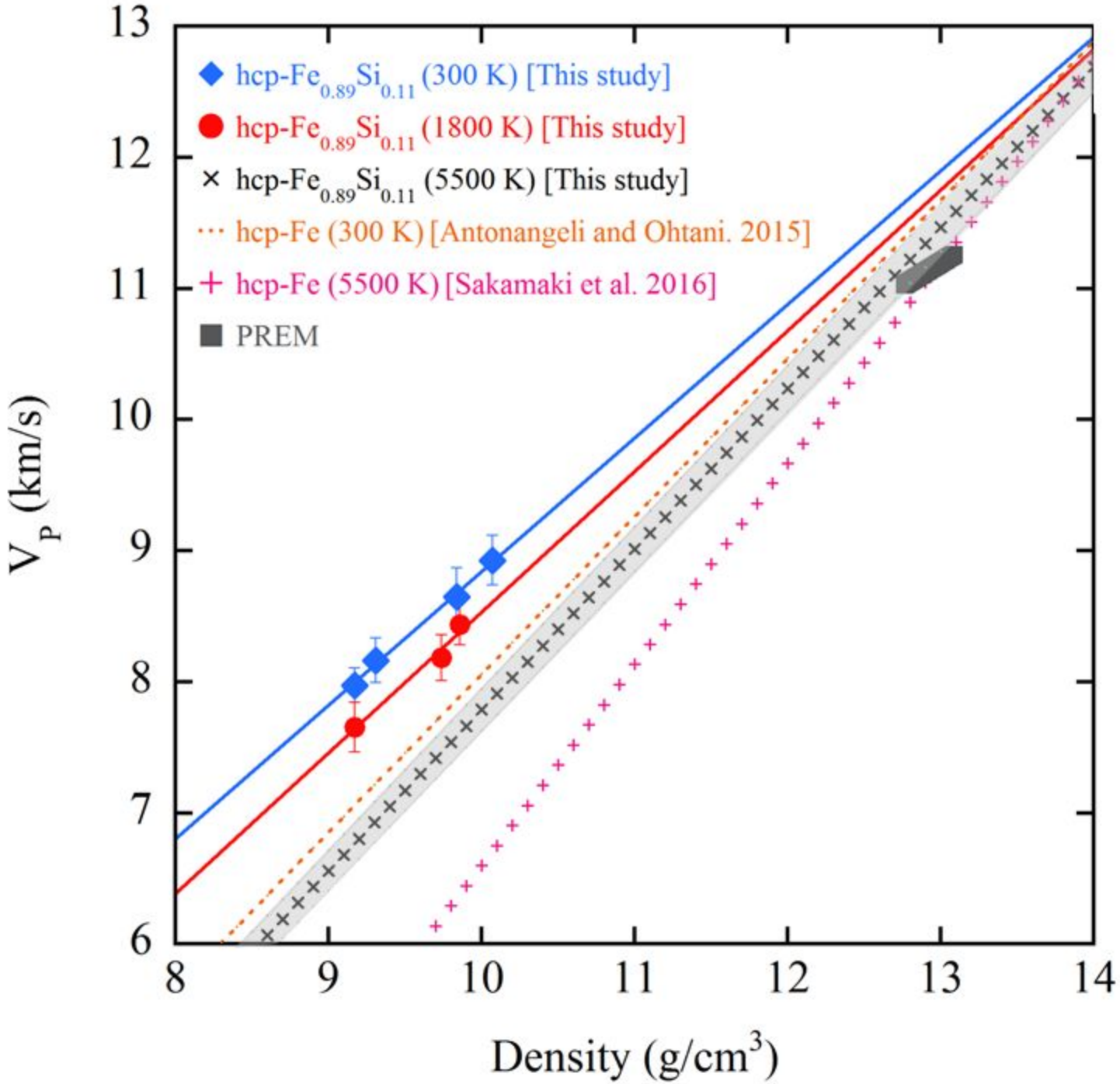
hcp-Fe0.89Si0.11 (300 K) [This study]
hcp-Fe0.89Si0.11 (1800 K) [This study]
hcp-Fe0.89Si0.11 (5500 K) [This study]
hcp-Fe (300 K) [Antonangeli and Ohtani. 2015]
hcp-Fe (5500 K) [Sakamaki et al. 2016]
PREM
VP (km/s)
Density (g/cm3)
13
12
11
10
9
8
7
6
8
9
10
11
12
13
14

Figure 6

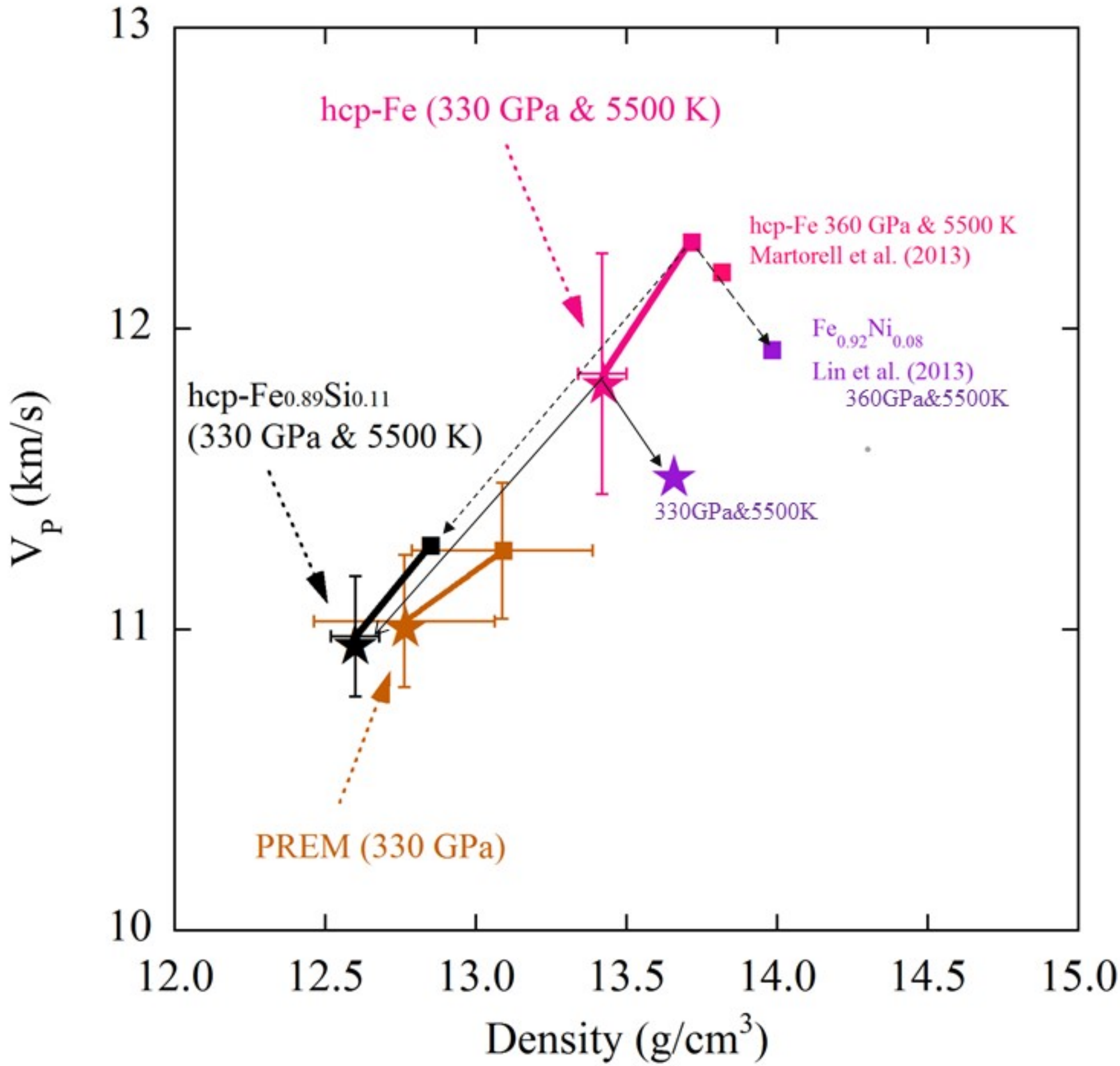
hcp-Fe (330 GPa & 5500 K)
hcp-Fe 360 GPa & 5500 K
Martorell et al. (2013)
$Fe_{0.92}Ni_{0.08}$
Lin et al. (2013)
360GPa&5500K
330GPa&5500K
hcp-$Fe_{0.89}Si_{0.11}$
(330 GPa & 5500 K)
PREM (330 GPa)
V_P (km/s)
Density (g/cm^3)
13
12
11
10
12.0
12.5
13.0
13.5
14.0
14.5
15.0

Table 1. The experimental conditions, density (ρ) and sound velocity V_P at high pressure and temperature.

Pressure [GPa]	Temperature [K]	Density [g/cm^3]	V_P [km/s]
45±1	300	9.17±0.02	7.98±0.13
51±1	300	9.31±0.03	8.16±0.17
77±2	300	9.84±0.03	8.65±0.18
90±2	300	10.07±0.04	8.93±0.19
50±1	1800±200	9.16±0.02	7.65±0.19
78±2	1800±200	9.74±0.02	8.12±0.18
78±2	1800±200	9.74±0.03	8.18±0.16
84±2	1800±200	9.86±0.03	8.44±0.18